Nanoscale

Accepted Manuscript

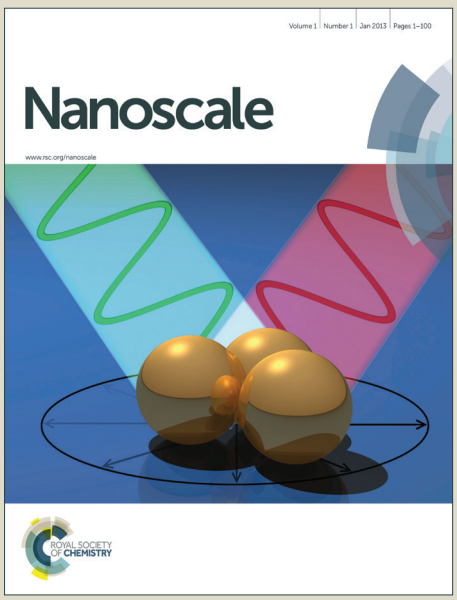

ROYAL SOCIETY OF CHEMISTRY

www.rsc.org/nanoscale

Table of Contents

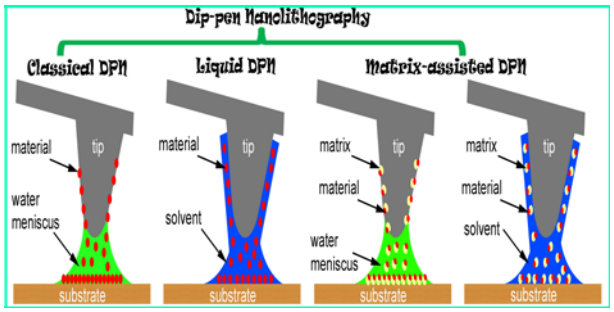

The focus of this review is on the development of three types of dip-pen nanolithography (classic, liquid, and matrix-assisted DPN) for studying the patterning of inorganic, organic, and biological materials onto a variety of substrates.

Classic, Liquid, and Matrix-assisted Dip-pen Nanolithography for Materials Research

Jian Zhong[*,†], *Gang Sun*[*,‡], *Dannong He*[†,§]

[†]National Engineering Research Center for Nanotechnology, Shanghai 200241, People's Republic of China

[‡]Department of Medical Imaging, Jinan Military General Hospital, No. 25 Shifan Road, Jinan, Shandong Province, People's Republic of China

[§]School of Materials Science and Engineering, Shanghai Jiao Tong University, Shanghai 200240, People's Republic of China

[*]E-mail: cjr.sungang@vip.163.com (G. S.) or jianzhongpku@hotmail.com (J. Z.).

Abstract: As a powerful atomic force microscopy-based nanotechnological tool, dip-pen nanolithography (DPN) has provided an ideal direct-write "constructive" lithographic tool that allows materials to be patterned from DPN tips onto a surface with high registration and sub-15-nm resolution. In the past decades, DPN has been enormously developed for studying the patterning of inorganic, organic, and biological materials onto a variety of substrates. The focus of this review is on the development of three types of DPN: classic, liquid, and matrix-assisted DPN. Such development mainly includes the following aspects: the comparisons of three types of DPN, the effect factors and basic mechanisms of three types of DPN, and the application progress of three types of DPN.

Keywords: dip-pen nanolithography (DPN), classic DPN, liquid DPN, matrix-assisted DPN

1. Introduction

Stable, precisely controlled and reproducible micro- and nano-patterning technology has become an exciting challenge in recent years owing to its widely potential applications in a number of fields ranging from semiconductor industry to medicine and to biotechnology.[1-2] A wide variety of techniques have been developed and explored to fabricate nano-to-microscale architectures including traditional photolithography,[3-4] electron-beam lithography,[5-6] microcontact/nanocontact printing,[7-9] nanoimprint lithography,[10-11] and scanning probe lithography (SPL).[12] Among these methods, SPL provides both high resolution and in situ imaging capabilities, and therefore, it has attracted increasing attentions from scientists in the academic field.[13]

SPL is a popular high resolution patterning technique that uses a sharp tip to pattern nano-to-microscale features onto a surface.[14-16] Currently, atomic force microscopy (AFM) and scanning tunneling microscopy (STM) are the two most popular scanning probe microscopy techniques those are used for SPL. AFM can be applied for morphological, mechanical, electrical, thermal, and magnetic characterization of either conductive or nonconductive surfaces in wider environment range from high vacuum to air to liquid environments. It has been successfully applied to image and manipulate single atoms,[17-18] to image molecules on surface,[19] to manipulate molecules on surface,[20-23] to image surface features,[24-25] to measure the kinetic parameters of molecule-molecule interactions,[26] to mechanically fabricate 3D nanoarchitectures,[27] and to visualize the molecular dynamic interaction.[28-29] While STM has a higher resolution, nevertheless, it only can be carried for conductive surfaces in high vacuum environment.[30] Therefore, AFM has a much wider application range over STM for lithography.

Many AFM-based techniques have been developed to fabricate nano-to-microscale architectures, including dip-pen nanolithography (DPN),[31-33] electrochemical AFM nanolithography,[34] nanografting,[35] and nanoshaving (mechanical scratching).[36] Among these

AFM-based lithography methods, DPN is the only 'constructive' lithographic tool that uses scanning probe to print materials onto a surface with high registration and high resolution,[33] and is also the only lithographic tool that can create arrays with hundreds of features by using a tip array (named as parallel DPN).[37] Therefore, DPN has been widely used for the patterning of a large variety of materials such as small organic molecules,[38-40] carbon nanotubes,[41] nanoparticles,[42-44] polymers,[45-46] proteins,[12, 47] peptides,[48-50] nucleic acids,[51-52] viruses,[53-54] and bacteria.[55]

DPN was first reported by Mirkin's group and was used to fabricate alkanethiol nanostructures on a gold surface in 1999.[31] It is a nanotechnology analog of the dip pen. An AFM tip or an array of AFM tips acts as a pen, which is coated with materials acting as an "ink". DPN uses the "ink"-coated "pen" to deposit "ink" on a substrate of interest acting as a "paper".

The deposition strategies of the objective materials by DPN can be categorized into two types: [56] direct DPN methods and indirect DPN methods. In the direct DPN methods, the inks are the objective materials. The objective materials are directly deposited onto a substrate. In the indirect DPN methods, the inks are not the objective materials. The inks are patterned on a substrate as linkers, masks, or molecular precursors on a substrate, and then the objective materials were associated to the linkers, immobilized on the unmasking areas, or produced from the molecular precursors on the substrate.

According to the ink state and the ink composition, DPN can be mainly categorized into three types: classic, liquid, and matrix-assisted DPN. Though DPN's developments, applications, challenges, and the comparisons with other techniques have been reviewed recently in several papers.[33, 56-63] The comparisons of the three types of DPN have not been reviewed yet. Considering the essential differences in the molecular transport and deposition, it is important to review the research and application progress of the three types of DPN. Therefore, in this article, we will focus on the ink state and the ink composition, and review

the developments of classic, liquid, and matrix-assisted DPN. The review will be divided into three sections: (i) comparisons of three types of DPN, (ii) effect factors and basic mechanisms of three types of DPN, (iii) application progress of three types of DPN.

2. Comparisons of classic, liquid, and matrix-assisted DPN

According to the ink state and ink composition, DPN can be categorized into three types: classic, liquid, and matrix-assisted DPN (Figure 1). In the classic DPN, small molecule materials are attached onto a DPN tip by (i) thermal evaporation of ink molecules, [64] or (ii) dipping the tip into the material solution and then drying the tip to remove the solvent.[31] When the DPN tip contact the substrate, the small molecule materials (inks) are dissolved into a water meniscus that was formed between the DPN tip and the substrate, and then are transported from the water meniscus to the substrate.[31] In liquid DPN, the materials are directly dissolved in solvents and then are attached onto a DPN tip by dipping the tip into the material solution (ink solution). The ink solution is directly transported from DPN tip to a substrate when the tip put in contact with the substrate.[65] In matrix-assisted DPN, the materials are dissolved in a matrix carrier and then are attached onto a DPN tip by dipping the tip into the material-matrix solution (ink solution). The material-matrix transport from DPN tip to a substrate can be mainly categorized into two types: (i) Similar to classic DPN, the material-matrix molecular ink is formed after drying the material-matrix solution, and then the material-matrix mixture is transported from DPN tip to a substrate via water meniscus.[66] (ii) Similar to liquid DPN, the ink solution is directly transported from DPN tip to a substrate when the tip put in contact with the substrate.[67]

The comparisons of the three types of DPN were summarized in Table 1. From Table 1, it is apparent that there are obvious differences among these three types of DPN. Classic DPN could be used to transport dried water-soluble inks (alkane thiols, silanes, etc) to their corresponding substrates (gold, glass, silicon, etc). The feature size of the deposited materials using classic DPN could be 15-2000 nm. Liquid DPN could be used to transport material

(inorganic, organic, and biological materials) solution to any flat substrate. The feature size of the deposited materials using liquid DPN could be 50 nm to several microns. Matrix-assisted DPN is mainly used to transport objective materials (nanoparticles, proteins, DNAs, and etc) in matrix to any flat substrate. The feature size of the deposited materials using matrix-assisted DPN could be 20 nm to several microns.

Table 1. Comparisons of classic, liquid, and matrix-assisted dip-pen nanolithography

	Classic DPN	Liquid DPN	Matrix-assisted DPN
Inks	Molecule inks	Material solution	Material-matrix solution
Transport medium	Water meniscus	Material solution	Water meniscus or Material-matrix solution
Material examples	Alkane thiols written to gold, Silanes (solid phase) written to glass or silicon Metal ions Peptides Water-soluble nanoparticles	Inorganic materials (nanoparticles, inorganic salts), Organic materials (organic molecules and organic salts, polymers), Biological materials (proteins, DNAs, lipids, bacterial cells, viruses)	Inorganic salts, Nanoparticles Protein, DNA
Ink medium (matrixes-solvents)	----	Solvents: Aqueous phase (water, phosphate-buffered saline, phosphate buffered saline with commercial protein carrier buffer), Organic phase (dimethylformamide, dimethylformamide/glycerol, butanol, hexane, toluene, chloroform), Aqueous-organic mixture (water/dimethylformide/glycerol)	Solvents(toluene, water, tricine buffer) Matrixes (small organic molecules, polymers, polysacchrides, proteins)
Feature size	15-2000 nm	50 nm -several microns	20 nm – several microns
Multiplex deposition	Yes	Yes	Yes
Effect factors to the deposition rate	Ink (chain length, ink surface coverage), DPN tip (shape), Water meniscus, Substrate (roughness), Environmental factors (organic vapor, temperature, humidity)	Interfacial energy between the ink and the surface, Thickness of the ink layer on the wall of the tip, Viscosity of the liquid	Same to classic or liquid DPN
Effect factors to the feature	Deposition rate of the ink,	Deposition rate of the liquid, Tip/substrate dwell time	Same to classic or liquid DPN

size	Tip/substrate dwell-time

3. Effect factors and basic mechanisms of three types of DPN

Due to the widely successful application of DPN in the patterning of inorganic, organic, and biological materials, the understanding of the fundamental mechanisms and their effect factors becomes critical. There are three types of basic research methods for studying the effect factors and basic mechanisms of DPN: (i) Experimental methods. They are mainly used to investigate the effect factors on the DPN process by analyzing the relationships between the effect factors and the deposited features. (ii) Theoretical mathematical models to fit the experimental results. The theoretical mathematical models try to incorporate key effect factors to generate a model for the understanding of the DPN process. The best fit mathematical models showed the relationships between the deposition features and the effect factors. These mathematical models can provide powerful framework to analyze and control the DPN progress. (iii) Molecular dynamics (MD) simulations. The molecular ink deposition in DPN is very quick and most of the fundamental properties are extremely difficult to obtain from experiments. Therefore, MD simulations are widely employed to analyze the detailed mechanical and thermodynamic information at the atomic level. MD is a powerful atomic modeling technique for studying molecular behaviors at the nanometer level. MD simulations could be used to investigate the DPN process that considers the complex physical and chemical interactions between molecules at molecular level in the DPN process.

The ink state of DPN can be mainly classified into two types: (i) dried molecular inks for classic and matrix-assisted DPN; (ii) liquid inks for liquid and matrix-assisted DPN. Therefore, the ink transport models of DPN can be classified into two types: molecular diffusion model for molecular ink transport and fluid flow model for liquid ink transport.[63] Only experimental methods were used to understand the basic mechanism of fluid flow model. The effect factors to the deposition rate mainly include the interfacial energy between the ink

and the surface, the thickness of the ink layer on the wall of the tip, and the viscosity of the liquid.[68] The effect factors to the feature size mainly include the deposition rate of the liquid and the tip/substrate dwell time.

Up to now, experimental methods, theoretical mathematical models to fit the experimental results, and MD simulations were mainly used to study the basic mechanism of molecular diffusion model in classic DPN. Therefore, we mainly summarized the recent progress of the effect factors and basic mechanisms of classic DPN in this section.

To study the effect of the molecule inks on the classic DPN deposition, Fang and co-workers [69] evaluated the effect of chain length of alkanethiol self-assembly monolayers in DPN using MD simulations. The simulation results clearly revealed that the molecular transfer ability of DPN strongly correlated with the chain length of alkanethiols. Giam et al. [70] experimentally presented a quantitative model that ink deposition rates were governed by ink surface coverage on the DPN tip. The limiting step in the entire DPN process was the dissolution of ink into the meniscus because that the deposition of alkanethiols from the meniscus to the gold substrate was a rapid process.

The effects of the DPN tip on the DPN deposition were also studied. Jang and co-workers [71] investigated the tip effects on classic DPN results by MD simulation. They compared the effects of two different tips, a quill type spherical tip and a cylindrical tip like a fountain pen, and found that a substantial variation in the tip did not induce any obvious change. Later, Fang and co-workers [72] studied the effects of the type of probe tip on the DPN array by MD simulation. The molecular transfer ability of the conical tip array was better than that of the pyramidal tip array. The number of transferred chains increased with the decrease of the tip distance for the conical tip array, whereas it decreased for the pyramidal tip array.

To obtain a fully molecular picture of the meniscus, Jang and co-worker [73] studied the structure and role of a nanoscale water meniscus in the classic DPN of alkanethiol SAM formation by MD simulation. The results showed the shape of the meniscus fluctuated and

could be quite asymmetric when the tip was in close contact with a surface. In addition, alkanethiols moved on the surface of, not into the interior of, the water meniscus.

The effect of the substrate on the DPN deposition was also studied. Fang and co-worker [74] investigated the effect of substrate roughness on the DPN process. The molcular transfer ability was optimum for deposition on a smooth surface.

The effect of environmental factors on DPN deposition has also been investigated. Mirkin and coworkers [75] investigated the effects of organic vapor on deposition rate and feature size of alkanethiol nanostructures in classic DPN. The presence of organic vapor increased the deposition rate and the feature size, in some cases by an order of magnitude. It points toward a way of working with water-incompatible molecules and materials. Fang and co-workers [76] studied the mechanisms of molecular transference, pattern formation, and mechanical behavior in DPN using MD simulation and found that molecular transfer ability depends on temperature. Fang and co-worker [77] also investigated the effects of humidity and deposition temperature on the laser-assisted DPN process. The number of transferred molecules increased with the increase of humidity. The surface binding energy decreased and the diffusion coefficient of ink molecules increased with the increase of humidity and deposition temperature. The DPN transfer efficiency could be significantly enhanced by increasing the laser heating rate.

According to the above reviews, the molecule ink (chain length, ink surface coverage), the DPN tip (shape), the water meniscus, the substrate (roughness), and environmental factors (organic vapor, temperature, and humidity) could affect the deposition rate in the classic DPN process.

Some ink diffusion/transport models were suggested to help the researchers to understand the basic mechanisms of classic DPN. A model was suggested by Saha, et al. to describe the whole classic DPN process.[78] In this model, the transport process of classic DPN can be divided into three steps (Figure 2). The first step is ink dissolution into the meniscus at the tip-

meniscus interface, the second step is ink diffusion through the meniscus to the meniscus-substrate interface, and the third step is surface transport of ink from the meniscus-substrate interface to the substrate surface. This ink transport mechanism of classic DPN is different to those of liquid DPN and matrix-assisted DPN, where ink (material in solvent or matrix) is directly transported from tip to substrate.

The ink diffusion rate from tip to substrate was typically assumed to be constant in the surface diffusion model from DPN tip to substrate. This works well for dot writing but fails for line writing. Culpepper and co-worker [79] presented a surface diffusion model for DPN line writing based on a constant tip-concentration assumption. It was more accurate than the constant flow rate approach, but it overestimated the flow rate at higher writing speeds. Later, Culpepper and co-worker [78] suggested a comprehensive ink transport model that unifying the constant rate and constant tip-concentration approaches and reduced errors in line width prediction in DPN line writing by up to 30%.

The ink transport models for the ink transfer from the meniscus-substrate interface to the substrate surface were also explored and proposed. In 2001, by using theoretical mathematical models to fit the results, Jang et al [80] suggested a hopping down model for the self-assembly of alkanethiol ink molecules on substrate in DPN (Figure 3b). When the ink-coated DPN tip was put into contact with a substrate, ink molecules were transported from the tip to the substrate to form a multiplayer droplet. A molecule on top (shaded circles) moved over the bottom layer (open circles) and hopped down to the bare substrate. The molecule-substrate binding was assumed to be irreversible extremely strong (generally chemical binding) and therefore the molecules got trapped. However, the real situation is that, although alkanethiols strongly stick to the gold surface, they can move rather easily from one of hollow sites of Au (111) to another. To overcome this weakness, based on the findings of MD simulations, Jang and co-worker [81] proposed a new serial pushing model for self-assembly monolayer pattern in classic DPN where the molecular vertical movements were severely restricted and the

molecular lateral movements were relatively facile after the molecule-substrate binding (Figure 3b). In the serial pushing model for SAM formation, the alkanethiols dropped from the tip (shaded circles) pushed a molecule on the substrate (open circles) out of its original position, and the alkanethiols on the substrate were in turn pushed to the periphery. Later, to illustrate the dendritic growth of an organic monolayer in classic DPN, Jang and co-workers [82] suggested a simple random-walk model that combined hopping down model and serial pushing model (Figure 3). This model accurately reproduced MD simulations for the DPN of nonpolar molecules on gold-like substrates. By changing the directional conherence, this model could reproduce a variety of patterns such as circles, hexagons, and dendrites. It is a significant progress over the previous models of DPN and can be implemented easily in the simulation of DPN with a tip moving over a substrate.

4. Application of three types of DPN

Classic, liquid, matrix-assisted DPN have been widely used to directly or indirectly pattern inorganic, organic, and biological materials. In this section, we will review the application of classic, liquid, matrix-assisted DPN for the direct or indirect deposition of the materials.

4.1. Classic DPN

During the classic DPN process, the dried molecular inks that coated on the DPN tip dissolved and diffused in the meniscus, and then transported from the meniscus to the substrate. The molecular inks are typically water-soluble materials such as alkathiols, metal ions, and peptides.

4.1.1. Alkanethiol materials

The DPN-generated alkanethiol patterns can be used as an etch mask for the deposition of other materials. Bao and co-workers [83] used DPN to deposit 16-mercaptohexadecanoic acid (MHA) pattern as an etch resist mask to fabricate monolayer graphene flakes and Au electrodes (Figure 4). Monolayer graphene device with two gold electrodes were formed. It provides a new method for fabricating nanoscale graphene devices that was generally

fabricated by electron-beam lithography. Later, Bao and co-workers [84-85] used DPN to deposit MHA pattern as an etch resist mask to parallelly fabricate Au electrode arrays on single-walled carbon nanotubes (SWNTs). These works verifies that DPN could be applied to generate high-quality electrodes in a parallel fashion with mild, relatively cheap, simple processing steps. It was the first time numerous SWNTs were electrically characterized using short-channel devices and increased the possibility of a number of practical application of SWNT devices.

The DPN-generated alkanethiol patterns can be used as a deposition mask for the deposition of other materials. Valiokas and coworkers [86] patterned MHA on the Au substrate as a deposition mask by DPN. The unmasking area was passivated by a hydrophobic SAM of either hexadecanethiol or a longer compound containing hexaethylene glycol and alkyl chain portions. The patterned substrate was used to prepare submicrometer-sized PEG hydrogel patterns by self-initiated photografting and photopolymerization. The patterned hydrogel could be carboxylated and functionalized to obtain protein density nanoarrays so that making it possible for a further exploration of single-cell manipulation and analysis.

The alkanethiol patterns can be used as a linker for the deposition of objective materials. Wang and coworker [87] used DPN to pattern MHA SAM on a gold surface for subsequent electroless deposition of copper nanostructures. This provides a new and simple strategy to fabricate metal-SAM-metal junctions within nanoscale dimensions.

To sum up, classic DPN can be applied to pattern the alkanethiol patterns, which can be used as an etch mask, a deposition mask, a linker, or etc. for the deposition of objective materials.

4.1.2. Metal ion materials

Metal ions can be patterned on a substrate by classic DPN. The metal ion patterns can be used as molecular linkers, catalyst precursors, and etc. Subramaniam and co-workers [88] used DPN to directly deposit metal Ni ions on NTA-terminated SAM for the immobilization of

His-tagged proteins (Figure 5). This is the first report of direct patterns of metal ions with lithographic techniques as a template for protein immobilization. Kang et al. [89] used DPN to deposit metal Ni ions on a silicon substrate to be catalyst precursors to synthesize carbon nanotubes in a plasma-enhanced chemical vapor deposition instrument. It demonstrates that DPN can be used to deposit catalyst precursors on a substrate for carbon nanotube synthesis with controlled location, properties, and density.

4.1.3. Peptide materials

Peptides can also be patterned on substrates by classic DPN. The patterned peptides can be used as biomolecular anchors, and etc. Ginger and coworkers [90] used DPN to pattern biotinylated engineered solid (gold or silica)-binding peptides on gold or silicon substrates. Using streptavidin-biotin interactions for fluorescent labeling, they confirmed the patterned peptides on the substrates could be used as biomolecular anchors to attach other materials to the solid substrates. It provides a DPN-generated nanopatterned peptide platform for the molecular linking in the field of diagnostic biosensors, nanophotonics, etc.

4.1.4 water-soluble nanoparticles

Dried water-soluble nanoparticles can also be patterned on substrates by classic DPN. Classic DPN was employed to pattern Pd nanocrystals,[91] Au nanocrystals,[44, 91] Fe_2O_3 nanocrystals,[92] and etc on several substrates such as mica, silicon, and etched silicon. The DPN tips were immersed into aqueous nanocrystal dispersion and then were dried in air. After that, dried water-soluble nanoparticles were coated onto the DPN tips as molecular inks.

4.2. Liquid DPN

In liquid DPN, the deposit materials are in appropriate solvents. The deposit materials are typically composed of inorganic materials (nanoparticles, inorganic salts), organic materials (organic molecules and organic salts, polymers), biological materials (proteins, DNAs, lipids, bacterial cells, viruses), and etc.

4.2.1. Inorganic materials

Liquid DPN can be applied to deposit many types of inorganic materials such as nanoparticles and inorganic salts.

Nanoparticles can be directly deposited on substrates by liquid DPN. Haaheim and coworkers [93] reported the first demonstration of submicrometer, sub-50-microΩ·cm conductive traces by direct deposition of a conductive Ag nanoparticle ink suspension on electrode patterns and multiple substrates (SiO_2, Kapton, Mica). It provides a new and reliable method for site-specific deposition of metallic materials for use in applications such as circuit repair, sensor element functionalization, gas sensing, and printable electronics.

Inorganic salts can be directly deposited on substrates by liquid DPN. Chandrasekhar and coworkers [94] used parallel DPN to pattern ferric nitrate in a mixture of water, dimethylformide, and glycerol on substrates. The patterned precursor catalysts were used for the fabrication of carbon nanotubes by chemical vapor deposition and resulted in a high yield of isolated carbon nanotubes. It provides an ideal way for carbon nanotube device fabrication.

4.2.2. Organic materials

Liquid DPN can be applied to deposit many types of organic materials such as organic molecules or organic salts, polymers, and etc.

Organic molecules or organic salts can be directly patterned on substrates by liquid DPN. Zhou et al. [95] used DPN to pattern Rhodamine 6G aqueous solution onto grapheme (Figure 6). The results showed Rhodamine 6G can be used to locally n-dope graphene in a controlled fashion. It highlights a path for controlling the electronic properties of graphene with nanoscale resolution in graphene devices by DPN and pointed out a direction to find a series of molecules that can be used to n- and p-dope graphene. Martinez-Otero et al. [96] used parallel DPN to pattern three different liquid inks of pH indicators (Oregon Green 514, fluorescein, and 5-carboxynaphthofluorescein) in 97% dimethylformamide and 5% glycerol to amino-silanized glass substrates by covalent attachments. The combined arrays allowed for sensitive, robust pH monitoring within the pH 3.0-9.0 range. This work proves the potential of DPN to

fabricate multi-analyte sensing platform at the micro- and nano-scale. Ruiz-Molina and coworkers [97] used DPN to pattern femtoliter droplets of organic ligands and/or inorganic metal ions onto regions of interest of substrate. The mixture of 1,3,5-benzenetricarboxylic acid with $Cu(NO_3)_2$ in dimethylformamide was used as the ink solution for the controlled growth of 1,3,5-benzenetricarboxylate crystals on two different SAMs made of MHA and 1-octadecanethiol (ODT). In addition, $[ErW_{10}O_{36}]^{9-}$ aqueous solution was used as ink to fabricate polyoxometalate-based arrays on Si/SiO_x substrate. These deposited liquid droplets can be used as nanoscale reactor vessels to fabricate arrays of single-crystals of metal-organic framework crystals and hollow capsules of magnetic polyoxometalates. It demonstrates that DPN could be used to pattern molecular-based coordination nanoarchitectures using tip-induced droplets as reactor vessels. Vapor phase polymerization is a relatively simple and rapid way for generating homogeneous conducting polymer layers. To scale down the polymerization method to submicron- and nano-scales, O'Connell et al. [98] firstly used DPN to pattern submicrometer scale oxidant (Fe(III) tosylate with a stabilizer in butanol) for vapor phase polymerization of conducting polymer poly(3,4-ethylenedioxythiophene) (PEDOT). It demonstrates that the in situ polymerization of a conducting polymer by the vapor phase could proceed within attoliter volumes of an oxidant ink.

Polymers can be directly patterned on substrates by liquid DPN. Hernandez-Santana et al. [99] used DPN to deposit PDMS prepolymer in hexane onto a SiO_2 substrate to fabricate dot array patterns. The PDMS prepolymer patterns were then cross-linked and bonded irreversibly to the substrate. PDMS is a popular material in the fabrication of microfluidic systems, so this method offers a significant advance in the ability to rapidly and easily produce PDMS features for BioMEMS application. Salaita and coworker [100] used DPN to pattern poly(diallyldimethylammonium chloride) (PDAC) in a mixture of water, ethanol, and ethylene glycol on the SiO_2 substrate. The DPN-generated PDAC pattern acted as a mask for the formation of phospholipid bilayer and can juxtapose mobile and immobile ligands in

supported lipid bilayer that simultaneously engaged the epidermal growth factor receptor (EGFR) and adhesion receptors on the cell surface. It offers significant advantages for the applications in studying supramolecular protein assemblies in living cells. Shin et al. [101] fabricated a graphene nanoribbon field effect transistor by combing DPN and polystyrene etching technique. The fabrication mainly included five steps. Firstly, polystyrene toluene solution was deposited onto a graphene sheet by DPN and then was dried and annealed to form polystyrene nanorods as an etching mask. Secondly, the graphene sheets except for that covered with polystyrene nanorods were removed by oxygen plasma. Thirdly, the polystyrene nanorods were removed by sonication and graphene nanoribbons were formed. Fourthly, DPN was used to deposit $PbCl_2$ solution at the left (right) end of the graphene nanoribbons, and then Pb nanodots were formed after solidification and anneal. Finally, DPN was used to deposit $AuCl_4$ solution over the Pb nanodots, and then Au nanowires were formed after solidification and anneal. The graphene nanoribbons field-effect transistor shows bipolar behavior with a high mobility and low operation voltage at room temperature. This work opens a possible way to fabricate the scalable, high-quality graphene nanoribbon field effect transistor.

4.2.3. Biological materials

Liquid DPN can be applied to deposit many types of inorganic materials such as proteins, DNAs, lipids, bacterial cells, viruses, and etc.[56, 61]

Proteins can be directly patterned on substrates by liquid DPN. Graham and coworkers [102] used DPN to pattern anti-prostate-specific antigen capture antibody in a mixture of phosphate buffered saline with commercial protein carrier buffer onto spin-coated nitrocellulose slides. The features produced on nitrocellulose were at least 20 times smaller than any features using other printing techniques and could be determined by standard fluorescence techniques. It is the first report of protein arrays on nitrocellulose using DPN. It demonstrates that DPN can be used to produce dense protein arrays on nitrocellulose for disease screening using standard

fluorescence detection. Further on, Graham and coworkers [103] used DPN to pattern capture protein (ERK2) in a mixture of phosphate buffered saline with commercial protein carrier buffer onto spin-coated nitrocellulose slides for the ERK2-KSR interaction studies on a physical scale. Though the overall assay efficiency was low, the arrays were reproducible and with low non-specific binding. This work proves it is possible to push protein analytical limits toward ultra-low (proteomic) concentration comparable to that are found in the cellular environment by DPN.

Lipids can be patterned on substrates by liquid DPN. Lenhert et al. [104] used parallel DPN to pattern lipids in chloroform on poly(methyl methacrylate) (PMMA) sheets (Figure 7). The produced photonic structures were composed of biofuctional lipid multilayers controllably with height ranging from 5 nm to 100 nm. This technique provides a new approach to fabricate and observe biomimetic nanosystems and is helpful for high-throughput biophysical analysis.

The direct deposition of large-sized materials remains a significant challenge for DPN technique. Bacterial cells and viruses were explored to be patterned on substrates by liquid DPN. Lim and coworkers [105] patterned adeno-associated viruses in phosphate-buffered saline from poly(2-methyl-2-oxazoline) (PMeOx)-coated tip to amine-functionalized SiO_2 substrate. It provides a direct and effective DPN method to fabricate patterns of large-sized viruses. It is the first time that direct DPN method is used to deposit large biomaterials. Later, Lim and coworkers [106] patterned bacterial cells in glycerol/tricine from PMeOx-coated tip to amine-functionalized SiO_2 substrate. By modulating the viscosity of the "ink", a single live bacterial cell array or arrays of layers of multiple live cells can be patterned on a solid surface. It is the first demonstration of DPN patterning of such large bacterial cells in a direct-write manner. These works demonstrate liquid DPN is possible to directly deposit large materials by a precise design of DPN tip coating.

4.3. Matrix-assisted DPN

In matrix-assisted DPN, the materials are in a matrix carrier. The material-matrix mixture could be transported from DPN tip to a substrate via molecular ink transport or liquid ink transport. Several materials have been explored to be the matrix for DPN deposition.

4.3.1. Small organic molecules as matrixes

Small organic molecules can be used as the matrixes for matrix-assisted DPN. In order to precisely control the pattern of metal nanostructures, Mirkin and co-workers [107] introduced alkanethiolates in toluene as a matrix for DPN of palladium ions onto a variety of substrates such as Si, Si/SiO_2, hexamethyldisilazane-coated hydrophobic Si, and polyimide (Figure 8). The deposited nanostructures showed an unusual characteristic of layer-by-layer assembly with precise control of both the height and feature size. After thermolysis, palladium nanoparticle pattern was formed. It provides a way to generate metal nanostructures on substrates by DPN with precise control of the location, height and feature size.

4.3.2. Polymers as matrixes

Polymers can be used as the matrixes for matrix-assisted DPN. Mirkin and co-workers [67] introduced poly(ethylene oxide)-b-poly(2-vinylpyridine) (PEO-b-P2VP) in deionized water as a matrix for DPN of $HAuCl_4$ or Na_2PtCl_4 on Si substrate (Figure 9). PEO-b-P2VP was chosen because the hydrophilic PEO block permits transport from tip to substrate while P2VP block coordinates metal ions. After the remove of the polymer matrix and the reduction of the metal ions by plasma treatment, pattern of single sub-10-nm metal nanoparticles was formed with precise control. It allows scientists to pattern single metal nanoparticles on surfaces and make it possible to integrate individual nanoparticles into desired spatial arrangements in micro- and nano-devices. Later, Mirkin and co-workers [108] used PEO-b-P2VP in deionized water as a matrix for DPN of $CdCl_2$ on Si or silicon nitride substrate. Then, the patterned features were subsequently reacted with H_2S in the vapor phase and then were treated by plasma to remove the polymer matrix, the pattern of crystalline and luminescent binary semiconductor CdS nanoparticles were fabricated. The method opens an avenue for DPN to synthesize

multicomponent nanostructure for the research in the fields of catalysis, optoelectronics, and light-harvesting. Huang et al. [66] used PEG polymer as a matrix for nanomaterials (such as Au nanoparticles, Fe_3O_4 nanoparticles, C_{60}) deposition on substrates (such as metal, semiconducting, insulating, or organic surfaces) in DPN, which resulted in uniform patterns of nanomaterials. This method overcomes the solubility and surface interactions that previously inhibited uniform pattern fabrication by DPN. Arrabito et al. [109] used parallel DPN to pattern oligonucleotide glycerol-PEG(MW400-4000) solution on glass slides. The patterned DNA oligonucleotides were then used as capture strands for DNA-directed immobilization of oligonucleotide-tagged proteins. This work used PEG as a matrix for the transport of DNA from DPN tip to chemically activated glass surfaces.

4.3.3. Polysaccharides as matrixes

Polysaccharides can be used as the matrixes for DPN. Mirkin and coworkers [110] used agarose as a "universal" carrier to control the deposition process of proteins and oligonucleotides onto Codelink N-hydroxysuccinimide-ester activated glass substrates in DPN. The deposition rate systematically varied from 0 to 1.5 $\mu m^2 \cdot s^{-1}$ by controlling the concentration of an accelerator such as tricine buffer within the matrix. The agarose-assisted DPN provides a third handle to control deposition speed in addition to the traditional tip-substrate contact time and humidity used in conventional DPN. It could fabricate nanoarrays with the same deposition rates for different biomolecule and the agarose matrix might be easily washed away if biomolecules covalently bonded to the substrate, and thus it has a huge potential for parallel, multiplexed biomolecule pattern. Zhang and coworkers [111] used agarose as a matrix for DPN of proteinase K on a poly(L-lactic acid) (PLLA) film. After an enzymatic degradation process, the biodegraded nanopattern in PLLA film was obtained. The results suggest that chemical reactions induced by enzymes can be controlled by DPN at a nanoscale level, which is impossible in the traditional bulk system. Moreover, it provides an enzyme-

based negative nanolithography method for polyester materials to create biodegraded nanopatterns with controllable dimensions.

4.3.4. Proteins as matrixes

Proteins were also explored to be the matrix for DPN. Bellido et al. [112] used DPN to fabricate biological ferritin arrays. After a simple heat-treatment process, the protein shell of ferritins was removed and the encapsulated inorganic nanoparticles on the same location of the nanoarray were left. Consequently, nanoparticle nanoarray was formed. It demonstrates that DPN could be used to pattern bio-template proteins for the nanoparticle nanoarray fabrication.

5. Summary and outlook

To sum up, this review summarized the comparisons of three types of DPN, the effect factors and basic mechanisms of three types of DPN, and the recent application progress of classic, liquid, and matrix-assisted DPN. This review convincingly shows that the abilities of classic, liquid, and matrix-assisted DPN have for providing insights to nanofabrication of inorganic, organic, and biological materials. Classic, liquid, and matrix-assisted DPN can be widely applied to deposit different materials on substrate at different resolution. The three types of DPN will undoubtedly attract the attention of more and more materials scientists and engineers in the future.

It should be noted that classic, liquid, and matrix-assisted DPN has several challenges and should be worked in the future: (i) The fundamental mechanisms and effect factors of classic, liquid, and matrix-assisted DPN are crucial for designing new ink materials and adjusting the process parameters to pattern materials on substrates. However, they remain uncompletely clear. In the future work, it is necessary to understand the fundamental mechanisms by using experimental methods, molecular dynamics simulations, and theoretical mathematical models to fit the experimental results. (ii) DPN throughput is needed to be improved for the fabrication of a relatively large pattern. Multiple probes for parallel processing and DPN tip

speed increasing are possible solutions and have been explored.[60] In addition, New DPN and SPL techniques have been developed to overcome the throughput limitation.[113-115] (iii) Biological molecules such as proteins and lipids carry out their structure and function under water, the ability to deposit and image them under water by DPN is particularly desirable. Up to now, AFM lithography has already been explored to deposit small biomolecules such as lipids [116] and biomacromolecules such as silk fibroin [117] under water. In the coming decade, it is important to address these challenges and continue to work on the application of classic, liquid, and matrix-assisted DPN for the patterning inorganic, organic, and biological materials.

Acknowledgments:

This research has been supported by research grants from the National Natural Science Foundation of China (51203024), the National High Technology Research and Development Program of China (863 Program 2013AA032203), the National Basic Research Program of China (2013CB932500), the Shanghai Pujiang Talent Program (12PJ1430300), and the Special Fund for Talents in Minhang District of Shanghai (2012).

References:

1. A. B. Braunschweig, F. Huo, and C. A. Mirkin, *Nat. Chem.*, 2009, **1**, 353-358.
2. D. Falconnet, G. Csucs, H. Michelle Grandin, and M. Textor, *Biomaterials*, 2006, **27**, 3044-3063.
3. A. Schwarz, J. S. Rossier, E. Roulet, N. Mermod, M. A. Roberts, and H. H. Girault, *Langmuir*, 1998, **14**, 5526-5531.
4. T. A. Martin, S. R. Caliari, P. D. Williford, B. A. Harley, and R. C. Bailey, *Biomaterials*, 2011, **32**, 3949-3957.
5. C. K. Harnett, K. M. Satyalakshmi, and H. G. Craighead, *Langmuir*, 2000, **17**, 178-182.
6. N. Glezos, K. Misiakos, S. Kakabakos, P. Petrou, and G. Terzoudi, *Biosens. Bioelectron.*, 2002, **17**, 279-282.
7. A. Bernard, J. P. Renault, B. Michel, H. R. Bosshard, and E. Delamarche, *Adv. Mater.*, 2000, **12**, 1067-1070.
8. H.-W. Li, B. V. O. Muir, G. Fichet, and W. T. S. Huck, *Langmuir*, 2003, **19**, 1963-1965.
9. J. Voskuhl, J. Brinkmann, and P. Jonkheijm, *Curr. Opin. Chem. Biol.*, 2014, **18**, 1-7.
10. V. N. Truskett, and M. P. C. Watts, *Trends Biotechnol.*, 2006, **24**, 312-317.
11. S. Shi, N. Lu, Y. Lu, Y. Wang, D. Qi, H. Xu, and L. Chi, *ACS Appl. Mater. Interfaces*, 2011, **3**, 4174-4179.
12. K.-B. Lee, J.-H. Lim, and C. A. Mirkin, *J. Am. Chem. Soc.*, 2003, **125**, 5588-5589.

13. S. Krämer, R. R. Fuierer, and C. B. Gorman, *Chem. Rev. (Washington, DC, U. S.)*, 2003, **103**, 4367-4418.
14. H. T. Soh, G. K. Wilder, and C. F. Quate, *Scanning Probe Lithography*. Kluwer Academic Publishers: Norwell, 2001.
15. X. Zhou, F. Boey, F. Huo, L. Huang, and H. Zhang, *Small*, 2011, **7**, 2273-2289.
16. R. Garcia, R. V. Martinez, and J. Martinez, *Chem. Soc. Rev.*, 2006, **35**, 29-38.
17. Y. Sugimoto, M. Abe, S. Hirayama, N. Oyabu, O. Custance, and S. Morita, *Nat. Mater.*, 2005, **4**, 156-159.
18. O. Custance, R. Perez, and S. Morita, *Nat. Nano.*, 2009, **4**, 803-810.
19. D. M. Czajkowsky, L. Li, J. Sun, J. Hu, and Z. Shao, *ACS Nano*, 2011, **6**, 190-198.
20. K. C. Neuman, and A. Nagy, *Nat. Methods*, 2008, **5**, 491-505.
21. M. Kim, C.-C. Wang, F. Benedetti, M. Rabbi, V. Bennett, and P. E. Marszalek, *Adv. Mater.*, 2011, **23**, 5684-5688.
22. F.-C. Zhang, F. Zhang, H.-N. Su, H. Li, Y. Zhang, and J. Hu, *ACS Nano*, 2010, **4**, 5791-5796.
23. Y. Zhang, X. Hu, J. Sun, Y. Shen, J. Hu, X. Xu, and Z. Shao, *Microsc. Res. Tech.*, 2011, **74**, 614-626.
24. R. B. Pernites, M. J. L. Felipe, E. L. Foster, and R. C. Advincula, *ACS Appl. Mater. Interfaces*, 2011, **3**, 817-827.
25. L. Ke, S. C. Lai, H. Liu, C. K. N. Peh, B. Wang, and J. H. Teng, *ACS Appl. Mater. Interfaces*, 2012, **4**, 1247-1253.
26. E. Martines, J. Zhong, J. Muzard, A. C. Lee, B. B. Akhremitchev, D. M. Suter, and G. U. Lee, *Biophys. J.*, 2012, **103**, 649-657.
27. Y. Yan, Z. Hu, X. Zhao, T. Sun, S. Dong, and X. Li, *Small*, 2010, **6**, 724-728.
28. J. Zhong, W. Zheng, L. Huang, Y. Hong, L. Wang, Y. Qiu, and Y. Sha, *Biochim. Biophys. Acta - Biomembr.*, 2007., **1768**, 1420-1429.
29. J. Zhong, C. Yang, W. Zheng, L. Huang, Y. Hong, L. Wang, and Y. Sha, *Biophys. J.*, 2009., **96**, 4610-4621.
30. S. Chiang, *Chem. Rev. (Washington, DC, U. S.)*, 1997, **97**, 1083-1096.
31. R. D. Piner, J. Zhu, F. Xu, S. Hong, and C. A. Mirkin, *Science (Washington, DC, U. S.)*, 1999, **283**, 661-663.
32. X. Wang, X. Wang, R. Fernandez, L. Ocola, M. Yan, and A. La Rosa, *ACS Appl. Mater. Interfaces*, 2010, **2**, 2904-2909.
33. K. Salaita, Y. Wang, and C. A. Mirkin, *Nat. Nanotechnol.*, 2007, **2**, 145-155.
34. Y. Li, B. W. Maynor, and J. Liu, *J. Am. Chem. Soc.*, 2001, **123**, 2105-2106.
35. S. Xu, S. Miller, P. E. Laibinis, and G.-y. Liu, *Langmuir*, 1999, **15**, 7244-7251.
36. S. Xu, and G.-y. Liu, *Langmuir*, 1997, **13**, 127-129.
37. S. W. Lee, B. K. Oh, R. G. Sanedrin, K. Salaita, T. Fujigaya, and C. A. Mirkin, *Adv. Mater.*, 2006, **18**, 1133-1136.
38. G.-Y. Liu, S. Xu, and Y. Qian, *Acc. Chem. Res.*, 2000, **33**, 457-466.
39. Y. Zhang, K. Salaita, J.-H. Lim, and C. A. Mirkin, *Nano Lett.*, 2002, **2**, 1389-1392.
40. Z. Zheng, M. Yang, and B. Zhang, *J. Phys. Chem. C*, 2010, **114**, 19220-19226.
41. X. Zhou, F. Boey, and H. Zhang, *Chem. Soc. Rev.*, 2011, **40**, 5221-5231.
42. J. Zheng, Z. Chen, and Z. Liu, *Langmuir*, 2000, **16**, 9673-9676.
43. X. Liu, L. Fu, S. Hong, V. P. Dravid, and C. A. Mirkin, *Adv. Mater.*, 2002, **14**, 231-234.
44. W. M. Wang, R. M. Stoltenberg, S. Liu, and Z. Bao, *ACS Nano*, 2008, **2**, 2135-2142.
45. A. Noy, A. E. Miller, J. E. Klare, B. L. Weeks, B. W. Woods, and J. J. DeYoreo, *Nano Lett.*, 2001, **2**, 109-112.
46. X. Zhou, X. Liu, Z. Xie, and Z. Zheng, *Nanoscale*, 2011, **3**, 4929-4939.

47. L. S. Wong, C. V. Karthikeyan, D. J. Eichelsdoerfer, J. Micklefield, and C. A. Mirkin, *Nanoscale*, 2012, **4**, 659-666.
48. Y. Cho, and A. Ivanisevic, *J. Phys. Chem. B*, 2004, **108**, 15223-15228.
49. H. Jiang, and S. I. Stupp, *Langmuir*, 2005, **21**, 5242-5246.
50. R. Sistiabudi, and A. Ivanisevic, *J. Phys. Chem. C*, 2007, **111**, 11676-11681.
51. L. M. Demers, D. S. Ginger, S.-J. Park, Z. Li, S.-W. Chung, and C. A. Mirkin, *Science (Washington, DC, U. S.)* 2002, **296**, 1836-1838.
52. M. S. Onses, P. Pathak, C.-C. Liu, F. Cerrina, and P. F. Nealey, *ACS Nano*, 2011, **5**, 7899-7909.
53. J. C. Smith, K.-B. Lee, Q. Wang, M. G. Finn, J. E. Johnson, M. Mrksich, and C. A. Mirkin, *Nano Lett.*, 2003, **3**, 883-886.
54. C. L. Cheung, J. A. Camarero, B. W. Woods, T. Lin, J. E. Johnson, and J. J. De Yoreo, *J. Am. Chem. Soc.*, 2003, **125**, 6848-6849.
55. S. Rozhok, C. K. F. Shen, P.-L. H. Littler, Z. Fan, C. Liu, C. A. Mirkin, and R. C. Holz, *Small*, 2005, **1**, 445-451.
56. C.-C. Wu, D. N. Reinhoudt, C. Otto, V. Subramaniam, and A. H. Velders, *Small*, 2011, **7**, 989-1002.
57. D. S. Ginger, H. Zhang, and C. A. Mirkin, *Angew. Chem. Int. Ed.*, 2004, **43**, 30-45.
58. B. Basnar, and I. Willner, *Small*, 2009, **5**, 28-44.
59. Y. Li, H. Sun, and H. Chu, *Chem. Asian J.*, 2010, **5**, 980-990.
60. A. A. Tseng, *Nano Today*, 2011, **6**, 493-509.
61. H. Tran, K. L. Killops, and L. M. Campos, *Soft Matter*, 2013, **9**, 6578-6586.
62. G. R. Luis, and L. Jian, *J. Phys.: Cond. Matter*, 2009, **21**, 483001.
63. K. Brown, D. Eichelsdoerfer, X. Liao, S. He, and C. Mirkin, *Front. Phys.*, 2014, **9**, 385-397.
64. S. Rozhok, R. Piner, and C. A. Mirkin, *J. Phys. Chem. B*, 2002, **107**, 751-757.
65. K.-B. Lee, S.-J. Park, C. A. Mirkin, J. C. Smith, and M. Mrksich, *Science*, 2002, **295**, 1702-1705.
66. L. Huang, A. B. Braunschweig, W. Shim, L. Qin, J. K. Lim, S. J. Hurst, F. Huo, C. Xue, J.-W. Jang, and C. A. Mirkin, *Small*, 2010, **6**, 1077-1081.
67. J. Chai, F. Huo, Z. Zheng, L. R. Giam, W. Shim, and C. A. Mirkin, *Proc. Nat. Acad. Sci. U.S.A*, 2010, **107**, 20202-20206.
68. G. Liu, Y. Zhou, R. S. Banga, R. Boya, K. A. Brown, A. J. Chipre, S. T. Nguyen, and C. A. Mirkin, *Chem. Sci.*, 2013, **4**, 2093-2099.
69. C.-D. Wu, T.-H. Fang, and J.-F. Lin, *J. Colloid Interface Sci.*, 2011, **361**, 316-320.
70. L. R. Giam, Y. Wang, and C. A. Mirkin, *J. Phys. Chem. A*, 2009, **113**, 3779-3782.
71. D. M. Heo, M. Yang, H. Kim, L. C. Saha, and J. Jang, *J. Phys. Chem. C*, 2009, **113**, 13813-13818.
72. C.-D. Wu, T.-H. Fang, and T.-T. Wu, *Polymer*, 2012, **53**, 857-863.
73. H. Kim, L. C. Saha, J. K. Saha, and J. Jang, *Scanning*, 2010, **32**, 2-8.
74. C.-D. Wu, and T.-H. Fang, *Modelling Simul. Mater. Sci. Eng.*, 2011, **19**, 065008.
75. K. Salaita, A. Amarnath, T. B. Higgins, and C. A. Mirkin, *Scanning*, 2010, **32**, 9-14.
76. C.-D. Wu, T.-H. Fang, and J.-F. Lin, *Langmuir*, 2010, **26**, 3237-3241.
77. C.-D. Wu, T.-H. Fang, and T.-T. Wu, *J. Colloid Interface Sci.*, 2012, **372**, 170-175.
78. S. K. Saha, and M. L. Culpepper, *J. Phys. Chem. C*, 2010, **114**, 15364-15369.
79. S. K. Saha, and M. L. Culpepper, *App. Phys. Lett.*, 2010, **96**, 243105-243105-3.
80. J. Jang, S. Hong, G. C. Schatz, and M. A. Ratner, *J. Chem. Phys.*, 2001, **115**, 2721-2729.
81. H. Kim, and J. Jang, *J. Phys. Chem. A*, 2009, **113**, 4313-4319.
82. H. Kim, G. C. Schatz, and J. Jang, *J. Phys. Chem. C*, 2010, **114**, 1922-1927.

83. W. M. Wang, N. Stander, R. M. Stoltenberg, D. Goldhaber-Gordon, and Z. Bao, *ACS Nano*, 2010, **4**, 6409-6416.
84. S. Park, W. M. Wang, and Z. Bao, *Langmuir*, 2010, **26**, 6853-6859.
85. S. Park, H. W. Lee, H. Wang, S. Selvarasah, M. R. Dokmeci, Y. J. Park, S. N. Cha, J. M. Kim, and Z. Bao, *ACS Nano*, 2012, **6**, 2487-2496.
86. T. Rakickas, E. M. Ericsson, Ž. Ruželė, B. Liedberg, and R. Valiokas, *Small*, 2011, **7**, 2153-2157.
87. Y.-H. Chang, and C.-H. Wang, *J. Mater. Chem.*, 2012, **22**, 3377-3382.
88. C.-C. Wu, D. N. Reinhoudt, C. Otto, A. H. Velders, and V. Subramaniam, *ACS Nano*, 2010, **4**, 1083-1091.
89. S. W. Kang, D. Banerjee, A. B. Kaul, and K. G. Megerian, *Scanning*, 2010, **32**, 42-48.
90. J. H. Wei, T. Kacar, C. Tamerler, M. Sarikaya, and D. S. Ginger, *Small*, 2009, **5**, 689-693.
91. P. J. Thomas, G. U. Kulkarni, and C. N. R. Rao, *J. Mater. Chem.*, 2004, **14**, 625-628.
92. G. Gundiah, N. S. John, P. J. Thomas, G. U. Kulkarni, C. N. R. Rao, and S. Heun, *Appl. Phys. Lett.*, 2004, **84**, 5341-5343.
93. S.-C. Hung, O. A. Nafday, J. R. Haaheim, F. Ren, G. C. Chi, and S. J. Pearton, *J. Phys. Chem. C*, 2010, **114**, 9672-9677.
94. I. Kuljanishvili, D. A. Dikin, S. Rozhok, S. Mayle, and V. Chandrasekhar, *Small*, 2009, **5**, 2523-2527.
95. X. Zhou, S. He, K. A. Brown, J. Mendez-Arroyo, F. Boey, and C. A. Mirkin, *Nano Lett.*, 2013, **13**, 1616-1621.
96. A. Martinez-Otero, P. Gonzalez-Monje, D. Maspoch, J. Hernando, and D. Ruiz-Molina, *Chem. Commun.*, 2011, **47**, 6864-6866.
97. E. Bellido, S. Cardona-Serra, E. Coronado, and D. Ruiz-Molina, *Chem. Commun.*, 2011, **47**, 5175-5177.
98. C. D. O'Connell, M. J. Higgins, H. Nakashima, S. E. Moulton, and G. G. Wallace, *Langmuir*, 2012, **28**, 9953-9960.
99. A. Hernandez-Santana, E. Irvine, K. Faulds, and D. Graham, *Chem. Sci.*, 2011, **2**, 211-215.
100. Y. Narui, and K. S. Salaita, *Chem. Sci.*, 2012, **3**.
101. Y.-S. Shin, J. Y. Son, M.-H. Jo, Y.-H. Shin, and H. M. Jang, *J. Am. Chem. Soc.*, 2011, **133**, 5623-5625.
102. E. J. Irvine, A. Hernandez-Santana, K. Faulds, and D. Graham, *Analyst*, 2011, **136**, 2925-2930.
103. D. G. Thompson, E. O. McKenna, A. Pitt, and D. Graham, *Biosens. Bioelectron.*, 2011, **26**, 4667-4673.
104. S. Lenhert, F. Brinkmann, T. Laue, S. Walheim, C. Vannahme, S. Klinkhammer, M. Xu, S. Sekula, T. Mappes, T. Schimmel, and H. Fuchs, *Nat. Nano*, 2010, **5**, 275-279.
105. Y.-H. Shin, S.-H. Yun, S.-H. Pyo, Y.-S. Lim, H.-J. Yoon, K.-H. Kim, S.-K. Moon, S. W. Lee, Y. G. Park, S.-I. Chang, K.-M. Kim, and J.-H. Lim, *Angew. Chem. Int. Ed.*, 2010, **49**, 9689-9692.
106. J. Kim, Y.-H. Shin, S.-H. Yun, D.-S. Choi, J.-H. Nam, S. R. Kim, S.-K. Moon, B. H. Chung, J.-H. Lee, J.-H. Kim, K.-Y. Kim, K.-M. Kim, and J.-H. Lim, *J. Am. Chem. Soc.*, 2012, **134**, 16500-16503.
107. B. Radha, G. Liu, D. J. Eichelsdoerfer, G. U. Kulkarni, and C. A. Mirkin, *ACS Nano*, 2013, **7**, 2602-2609.
108. L. R. Giam, S. He, N. E. Horwitz, D. J. Eichelsdoerfer, J. Chai, Z. Zheng, D. Kim, W. Shim, and C. A. Mirkin, *Nano Lett.*, 2012, **12**, 1022-1025.
109. G. Arrabito, S. Reisewitz, L. Dehmelt, P. I. Bastiaens, B. Pignataro, H. Schroeder, and C. M. Niemeyer, *Small*, 2013, **9**, 4243-4249.

110. A. J. Senesi, D. I. Rozkiewicz, D. N. Reinhoudt, and C. A. Mirkin, *ACS Nano*, 2009, **3**, 2394-2402.
111. H. Li, Q. He, X. Wang, G. Lu, C. Liusman, B. Li, F. Boey, S. S. Venkatraman, and H. Zhang, *Small*, 2011, **7**, 226-229.
112. E. Bellido, R. de Miguel, J. Sesé, D. Ruiz-Molina, A. Lostao, and D. Maspoch, *Scanning*, 2010, **32**, 35-41.
113. W. Shim, A. B. Braunschweig, X. Liao, J. Chai, J. K. Lim, G. Zheng, and C. A. Mirkin, *Nature*, 2011, **469**, 516-520.
114. F. Huo, Z. Zheng, G. Zheng, L. R. Giam, H. Zhang, and C. A. Mirkin, *Science*, 2008, **321**, 1658-1660.
115. F. Huo, G. Zheng, X. Liao, L. R. Giam, J. Chai, X. Chen, W. Shim, and C. A. Mirkin, *Nat. Nano.*, 2010, **5**, 637-640.
116. S. Lenhert, C. A. Mirkin, and H. Fuchs, *Scanning*, 2010, **32**, 15-23.
117. J. Zhong, M. Ma, J. Zhou, D. Wei, Z. Yan, and D. He, *ACS Appl. Mater. Interfaces*, 2013, **5**, 737-746.

Figure 1

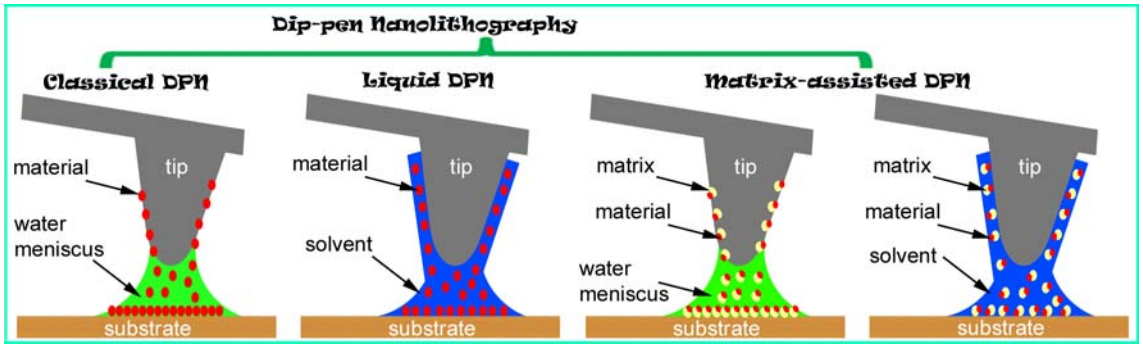

Figure 1. Schematics of classic, liquid, and matrix-assisted DPN.

Figure 2

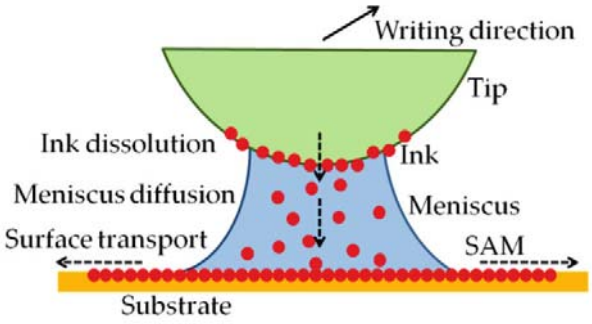

Figure 2. Ink transport process of classic DPN. Adapted with permission from reference [78] (Copyright 2010 American Chemical Society).

Figure 3

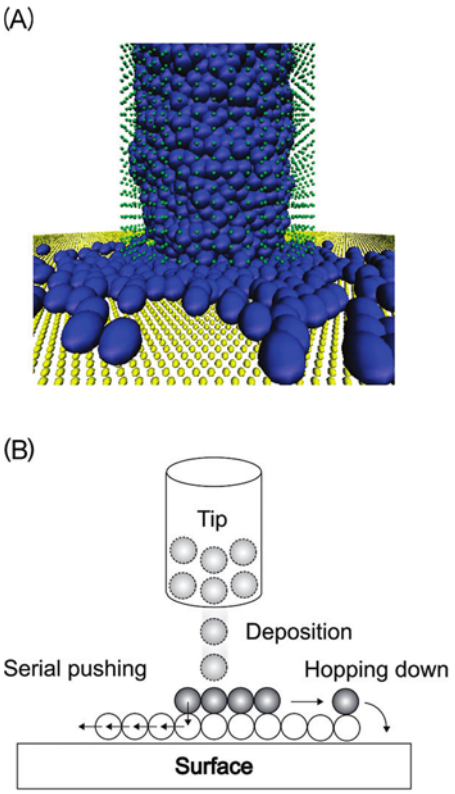

Figure 3. (A) MD simulation of classic DPN. Nonpolar spherical molecules are stacked on a cylindrical tip and later transported from the tip to form a monolayer onto the Au (111) surface. The tip and surface atoms are drawn smaller for clarity. (B) Random walk model of classic DPN. This model combined hopping down model and serial pushing model. Reprinted with permission from reference [82] (Copyright 2010 American Chemical Society).

Figure 4

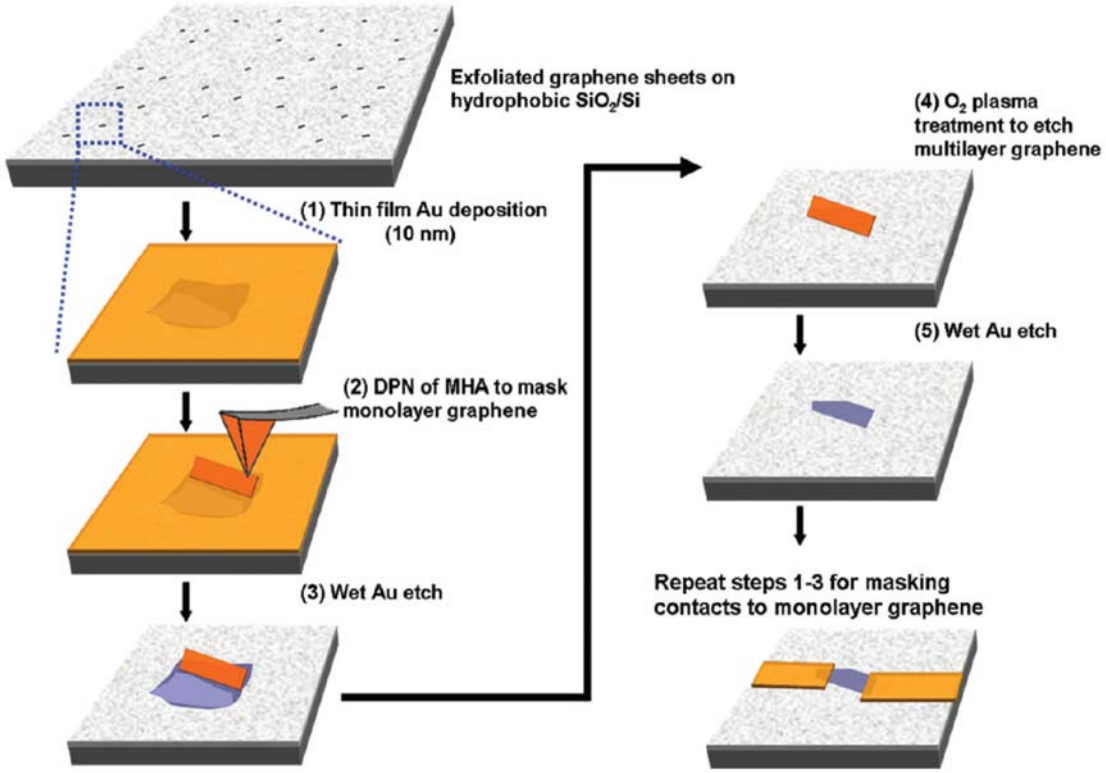

Figure 4. Schematic of grapheme device fabrication by classic DPN. In step 2, MHA mask was deposited on monolayer graphene (darker) rather than multilayer graphene (lighter). The unmasking Au film is etched away in step 3. The unmasking graphene regions and MHA mask are etched away in step 4. The Au film on the monolayer graphene is etched away in step 5, leaving a the monolayer graphene. Then the steps 1-3 were repeated to fabricate the macroscale electrodes. Reprinted with permission from reference [83] (Copyright 2010 American Chemical Society).

Figure 5

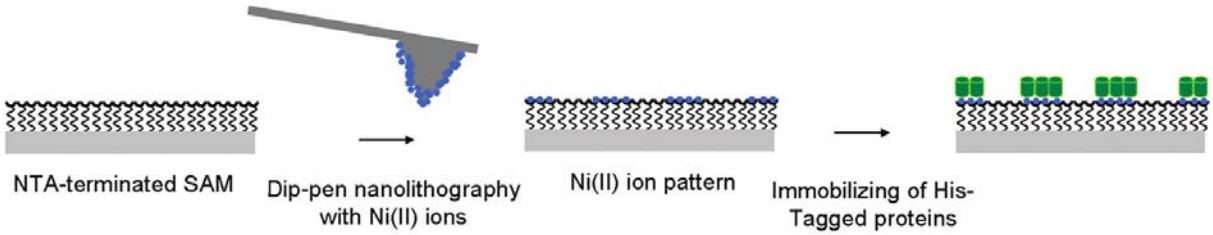

Figure 5. Fabrication of Ni(II) ion patterns onto NTA-terminated SAM by classic DPN to immobilize Hig-tagged proteins. Adapted with permission from reference [88] (Copyright 2010 American Chemical Society).

Figure 6

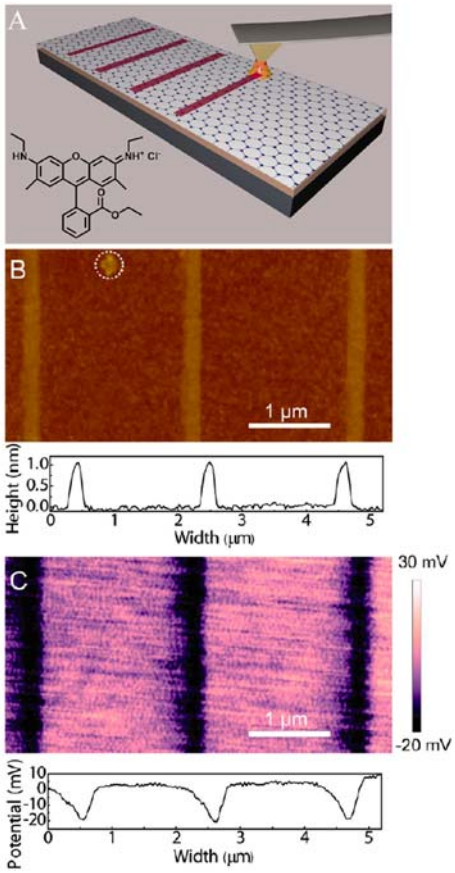

Figure 6. (A) Schematic of the the patterning of Rhodamine 6G (R6G) on grapheme by liquid DPN. (B) AFM height image and the average height profile of lines of R6G dimers patterned on graphene. (C) The surface potential image and the average surface potential profile of lines of R6G dimers patterned on graphene. Adapted with permission from reference [95] (Copyright 2013 American Chemical Society).

Figure 7

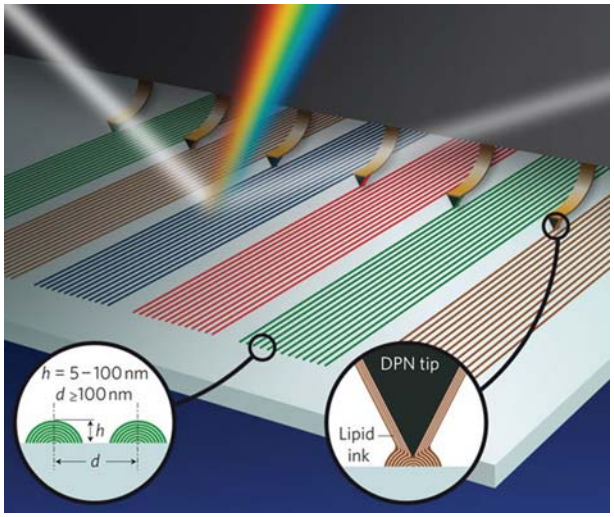

Figure 7. Schematic of lipid multilayer grating fabrication by liquid parallel DPN. Parallel DPN tip array is used to pattern multiple lipids simultaneously with controllable multilayer heights into arbitrary patterns. The diffracted light from the patterns can be used for high-throughput optical quality control without the need of fluorescence labels. Reprinted with permission from reference [104] (Copyright 2010 Nature Publishing Group).

Figure 8

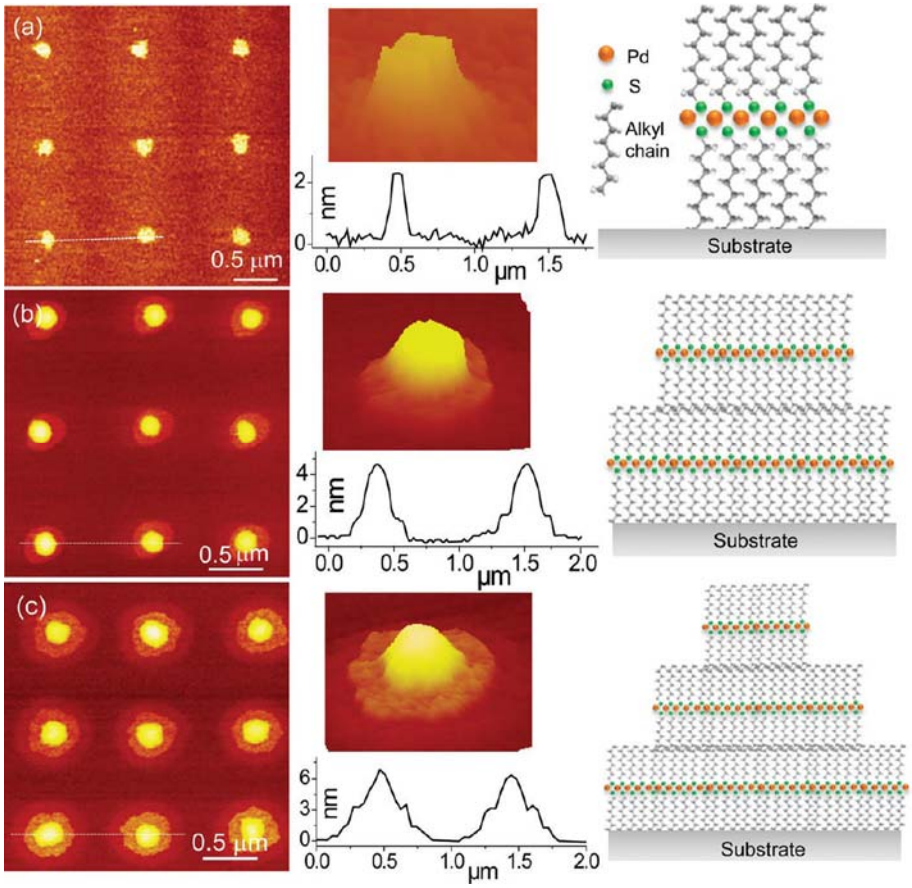

Figure 8. The patterning of Pd octylthiolate lamellar layers by DPN. (a-c): AFM height images of single layer, two layers, and three layers of Pd octylthiolate. The surface plots, the section analysis corresponding to the white lines in (a-c), and the schematic arrangement of Pd octalthiolate lamellae are shown alongside. Reprinted with permission from reference [107] (Copyright 2013 American Chemical Society).

Figure 9

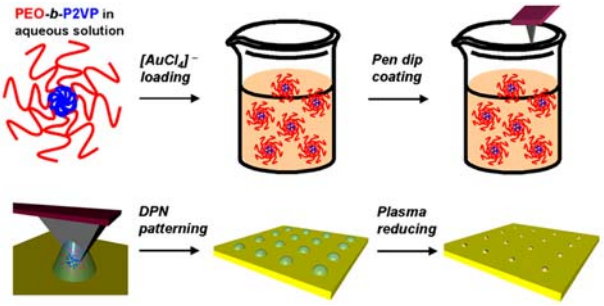

Figure 9. Schematic of the patterning of Au nanoparticles by matrix-assisted DPN. PEO-b-P2VP is used as the matrix. PEO-b-P2VP phase separated in aqueous solution to form P2VP cores (blue) surrounded by PEO coronas (red). P2VP cores coordinate AuCl4- ions. The hybrid ink is patterned onto the Si substrate. After the remove of the polymer matrix and the reduction of the metal ions by plasma treatment, a pattern of Au nanoparticle was formed. Reprinted with permission from reference [67] (Copyright 2010 National Academy of Sciences USA).